Theoretical Computer Science ••• (••••) •••–•••

Contents lists available at ScienceDirect

Theoretical Computer Science

www.elsevier.com/locate/tcs

Complex patterns in networks of hyperexcitable neurons

Craig Schindewolf [a,1], Dongwook Kim [a,2], Andrea Bel [b,3], Horacio G. Rotstein [a,*]

[a] Department of Mathematical Sciences, New Jersey Institute of Technology, Newark, NJ 07102, USA
[b] Department of Mathematics, Universidad Nacional del Sur, Bahía Blanca 8000, Buenos Aires, Argentina

ARTICLE INFO

Article history:
Received 9 January 2015
Received in revised form 17 April 2015
Accepted 1 May 2015
Available online xxxx

Keywords:
Neuronal networks
Synchronization

ABSTRACT

Complex patterns in neuronal networks emerge from the cooperative activity of the participating neurons, synaptic connectivity and network topology. Several neuron types exhibit complex intrinsic dynamics due to the presence of nonlinearities and multiple time scales. In this paper we extend previous work on hyperexcitability of neuronal networks, a hallmark of epileptic brain seizure generation, which results from the net imbalance between excitation and inhibition and the ability of certain neuron types to exhibit abrupt transitions between low and high firing frequency regimes as the levels of recurrent AMPA excitation change. We examine the effect of different topologies and connection delays on the hyperexcitability phenomenon in networks having recurrent synaptic AMPA (fast) excitation (in the absence of synaptic inhibition) and demonstrate the emergence of additional time scales.

1. Introduction

Neuronal networks of the brain display complex spatio-temporal patterns [1]. These patterns result from the cooperative activity of the participating neurons, the synaptic connectivity and the network topology [2,3]. The dynamics of individual neurons depend primarily on the nature and properties of the participating ionic currents whose combined activity generates the neuron's effective intrinsic time scales. Synaptic connectivity can be electrical (gap junctions) or chemical [4]. The latter, in turn, can be excitatory or inhibitory and operate at different time scales within a relatively large range. Network topologies depend on the brain area and the level of organization and include ring [5,6] (and references therein) and small-world network [7–10] connectivities.

While realistic neuronal networks include both excitation and inhibition, there are several aspects of the network dynamics that can be addressed by first understanding the dynamics of recurrently excited networks [8–13] and then investigating how recurrent inhibition affects the resulting patterns [12]. One such aspect is that of the hyperexcitability of neuronal circuits, which is one of the hallmarks of epileptic brain seizure generation [14,15]. Various hypotheses have been put forward to explain the generation of abnormal recurrent excitation including the lack of enough inhibition (dormant interneuron hypothesis) [16–24] and aberrant axonal reorganization of principal cells (e.g., mossy fiber sprouting in the dentate gyrus)

* Corresponding author.
E-mail address: horacio@njit.edu (H.G. Rotstein).

[1] Equal contribution. Current address: Department of Biological Sciences, New Jersey Institute of Technology, Newark, NJ 07102, USA.
[2] Equal contribution. Current address: Department of Mathematics, Atlanta Metropolitan State College, Atlanta, GA, USA.
[3] Equal contribution. This work was carried out during the author's visit to the Department of Mathematical Sciences, New Jersey Institute of Technology, Newark, NJ 07102, USA.

http://dx.doi.org/10.1016/j.tcs.2015.05.051
0304-3975/

(recurrent excitation hypothesis) [25–35]. Regardless of whether the net imbalance between excitation and inhibition results from decreased inhibition or increased excitation, the study of recurrently excited networks is key to understand how the network patterns transition between "normal" to hyperexcitable.

Synaptic excitation constitutes a positive feedback effect, and therefore increasing levels of the maximal AMPA synaptic conductance (G_{ex}) are expected to produce an increase in the spike (or firing) frequency f_{spk} at a rate that also increases with G_{ex} (Fig. 1-a1). However, synaptic excitation does not operate alone, but its net effect depends on its interaction with the intrinsic properties of the postsynaptic cell. As shown by us and other authors [12,13,36,37], this can result in some unintuitive effects. In [12] we have investigated the mechanism of hyperexcitability in medial entorhinal cortex layer II stellate cells motivated by experimental findings in [23,38]. We used self-excited cells mimicking a population of recurrently excited cells synchronized in phase. We showed that the firing frequency is maintained constant or slightly decreases for increasing values of the maximal synaptic conductance (G_{ex}) within some relatively large range, above which an abrupt increase in firing frequency to a significantly large value occurs (Fig. 1-b1). The firing frequency gradually increases for values of G_{ex} above this abrupt transition. The interaction between the decay time of excitation and the effective intrinsic time scales generated by the persistent sodium and the hyperpolarization-activated currents is crucial for this phenomenon. Synaptic inhibition acts as a switch between the two firing frequency regimes. In [13] we have carried out a thorough comparative study of the classes of models that produce these two qualitatively different types of behavior, and we have extended our results to minimal, two-cell network models.

The goal of this paper is to extend our results to larger networks. Specifically, we examine whether the gradual and abrupt transition between low and high firing frequencies generated by the two classes of models described above persist in larger, recurrently excited networks. In addition, we examine the similarities and differences between the patterns generated by these two classes of models in these larger networks. Finally, we investigate the role of synaptic delays in stabilizing the network activity in the high-frequency regime at lower spike frequencies than those for instantaneous synapses. Synaptic delays have been shown to play significant role in the generation of network coherent activity [39–47].

We use two models that are prototypical for the two modes of transitions between low and high firing frequencies: the integrate-and-fire (IF) model and the so-called $I_h + I_{Nap}$ model. The IF model has passive subthreshold dynamics (no active ionic currents) and exhibits gradual transitions (Fig. 1-a1). The $I_h + I_{Nap}$ model has persistent sodium and hyperpolarization-activated (h-) currents and exhibits abrupt transitions (Fig. 1-b1). For simplicity we focus on networks with ring topologies where each cell is only connected to its nearest neighbors. Our results provide the basis for the investigation of networks with more complex connectivity patterns and more general model types.

2. Methods

Neurons are modeled using the Hodgkin–Huxley (conductance-based) formalism [48]. The current-balance equation in the subthreshold voltage regime is given by

$$C\frac{dV}{dt} = -I_L - \sum_j I_{ion,j} + I_{app}, \tag{1}$$

where V is the membrane potential (mV), t is time (msec), C is the membrane capacitance ($\mu F/cm^2$), I_{app} is the applied bias (DC) current ($\mu A/cm^2$), $I_L = G_L(V - E_L)$ is the leak current, and $I_{ion,j}$ are ionic currents of the form

$$I_{ion,j} = G_j m_j^a h_j^b (V - E_j) \tag{2}$$

with activation and inactivation gating variables m_j and h_j respectively, maximal conductances G_j (mS/cm^2), reversal potentials E_j (mV), and constants $a \geq 0$ and $b \geq 0$. All gating variables x obey a first order differential equation of the form

$$\frac{dx}{dt} = \frac{x_\infty(V) - x}{\tau_x(V)} \tag{3}$$

where $x_\infty(V)$ and $\tau_x(V)$ are the voltage-dependent activation/inactivation curves and time-constants respectively.

The models used in this paper do not contain a biophysical description of the spiking dynamics, which is usually generated by the interplay of a transient sodium and delayed-rectifier potassium currents [4]. Instead, spikes are added artificially once the voltage has reached a threshold value V_{th}. The artificial spikes have the form $60\,e^{-2(t-t_{spk})}$ for $t \in [t_{spk}, t_{spk} + \Delta_{spk})$ where t_{spk} is a given spike time and Δ_{spk} is the spike duration, which was set to be equal to 1 msec. The variables V and x are reset at $t = t_{spk} + \Delta_{spk}$ to V_{rst} and x_{rst} respectively. In the leaky integrate-and-fire (IF) model V_{th} is part of the mechanism for spike generation. In contrast, the persistent sodium/h-current ($I_h + I_{Nap}$) model (described below) describes the onset of spikes and V_{th} only indicates their occurrence.

For the (IF) model [4] the subthreshold dynamics are described by eq. (1) with $I_{ion} = 0$. We used the following parameter values: $C = 1$, $E_L = -65$, $G_L = 0.025$, $V_{th} = -50$, $V_{reset} = -70$. Additional parameter values are provided in the corresponding figures.

The $I_h + I_{Nap}$ model is an adaptation of the reduced model derived in [49] from the fully spiking model introduced in [50]. The subthreshold dynamics are described by eqs. (1)–(3) with a persistent sodium current and an h-current given

Please cite this article in press as: C. Schindewolf et al., Complex patterns in networks of hyperexcitable neurons, Theoret. Comput. Sci. (2015), http://dx.doi.org/10.1016/j.tcs.2015.05.051

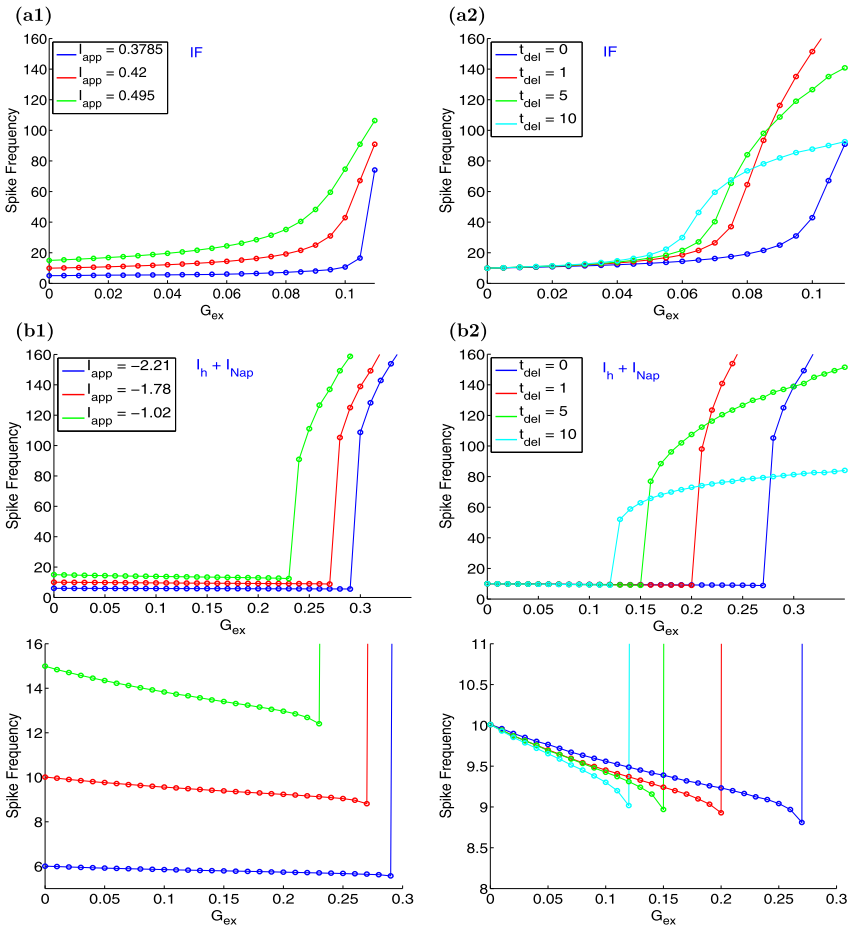

Fig. 1. Spike frequencies (f_{spk}) **for the self-connected IF and** $I_h + I_{Nap}$ **models as a function of the maximal synaptic conductance** G_{ex} **for representative values of** I_{app} **(left panels) and synaptic delay** t_{del} **(right).** (a) IF model. The values of f_{spk} for the uncoupled cell are: 5 Hz (blue), 10 Hz (red) and 15 Hz (green). (a1) $t_{del} = 0$. (a2) $I_{app} = 0.42$ (red in panel a1). We used the following parameter values $C = 1$, $E_L = -65$, $G_L = 0.025$ (b) $I_h + I_{Nap}$ model. The values of f_{spk} for the uncoupled cell are: 6 Hz (blue), 10 Hz (red) and 15 Hz (green). (a1) $t_{del} = 0$. (a2) $I_{app} = -1.78$ (red in panel a1). The bottom panels are magnifications of the top ones. We used the following parameter values $C = 1$, $G_L = 0.5$, $G_h = 1.5$, $E_L = -65$, $E_{Na} = 55$, $E_h = -20$. (For interpretation of the references to colour in this figure legend, the reader is referred to the web version of this article.)

by $I_{Nap} = G_p\, p\,(V - E_{Na}) = G_p\, p_\infty(V)\,(V - E_{Na})$ and $I_h = G_h\, r\,(V - E_h)$ respectively. The voltage-dependent activation/inactivation curves and time constants are given by $p_\infty(V) = 1/(1+e^{-(V+38)/6.5})$, $r_\infty(V) = 1/(1+e^{(V+79.2)/9.78})$, and $\tau_r(V) = 100$. We used the following parameter values: $C = 1$, $E_h = -20$, $E_{Na} = 55$, $E_L = -65$, $g_L = 0.5$, $V_{reset} = -80$ and $r_{reset} = 0$. Additional parameter values are provided in the corresponding figures.

The excitatory synaptic currents [4] (from neuron j to neuron k) considered in this paper are described by

$$I_{syn} = G_{j,k}\, S_j(t - t_{del})\,(V_k - E_{ex}) \tag{4}$$

where V_k is the voltage of the postsynaptic cell, $S_j(t)$ is the presynaptic variable, $G_{j,k}$ is the maximal synaptic conductance, $E_{ex} = 0$ is the excitatory reversal potential and t_{del} is the synaptic delay time. We will use the notation $G_{j,k} = G_{ex}$ when a uniform value for $G_{j,k}$ is used.

Synaptic variables $S(t)$ obey a kinetic differential equation of the form

$$\frac{dS}{dt} = N(V)\,\frac{(1-S)}{\tau_r} - \frac{S}{\tau_d}, \tag{5}$$

where $N(V)$ denotes the sigmoid function

$$N(V) = \frac{1 + \tanh(V/4)}{2} \tag{6}$$

and τ_r and τ_d are the rise and decay time constants respectively (msec). In this paper we focus on AMPA synaptic excitation with $\tau_r = 0.1$ and $\tau_d = 3$.

Please cite this article in press as: C. Schindewolf et al., Complex patterns in networks of hyperexcitable neurons, Theoret. Comput. Sci. (2015), http://dx.doi.org/10.1016/j.tcs.2015.05.051

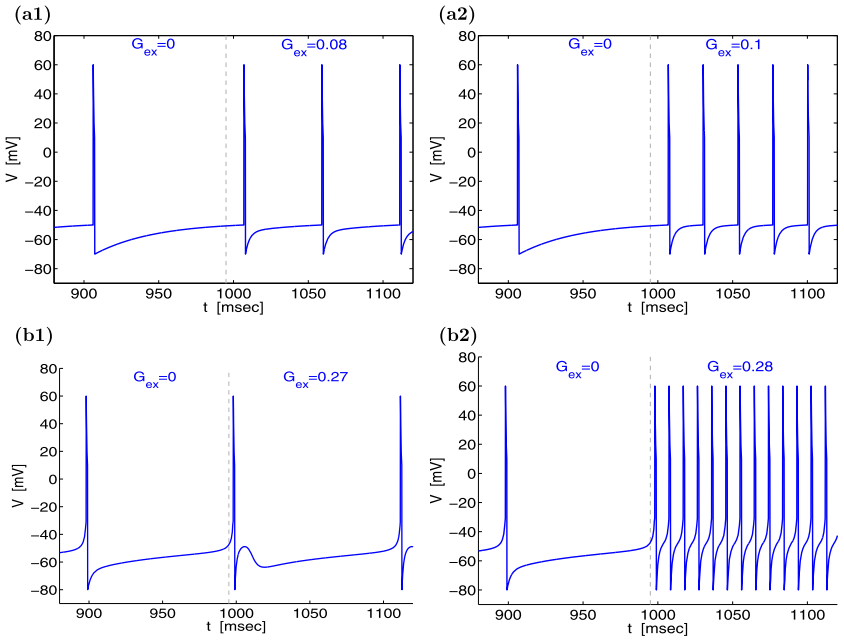

Fig. 2. Representative voltage traces for the IF and $I_h + I_{Nap}$ models before and after recurrent excitation is activated. The vertical gray line indicates the connection time. (a) IF model. We used the following parameter values $C = 1$, $E_L = -65$, $G_L = 0.025$, $I_{app} = 0.42$, $t_{del} = 0$. (b) $I_h + I_{Nap}$ model. We used the following parameter values $C = 1$, $G_L = 0.5$, $G_h = 1.5$, $E_L = -65$, $E_{Na} = 55$, $E_h = -20$, $I_{app} = -1.78$, $t_{del} = 0$.

The network population activity is measured using the following definition for the local field potential (LFP)

$$LFP(t) = \frac{1}{N}\sum_{k=1}^{N} S_k(t). \tag{7}$$

3. Results

3.1. Abrupt and gradual transitions between firing frequency regimes as the result of increasing levels of synaptic excitation in self-connected cells

Here we review previous results on the two qualitatively different modes of transition (gradual and abrupt) between the low and high (hyperexcitable) firing frequency regimes as the result of changes in the maximal AMPA synaptic conductance G_{ex} in minimal network models consisting of self-connected cells. The IF and $I_h + I_{Nap}$ models we use in this paper are prototypical for these two modes of transition. Our results are presented in Figs. 1-a1 (IF model) and Fig. 1-b1 ($I_h + I_{Nap}$ model). In all cases, the natural spike (firing) frequency (f_{spk}) for the isolated cells ($G_{ex} = 0$) increases with increasing values of I_{app}. Representative voltage traces (voltage time courses) for both models are presented in Fig. 2.

For the IF model (Fig. 1-a1), as G_{ex} increases, f_{spk} increases, first slowly and then faster. The G_{ex}–f_{spk} curves are smoother the larger I_{app}. In contrast, for the $I_h + I_{Nap}$ model (Fig. 1-b1), as G_{ex} increases, f_{spk} first decreases (see bottom panel) and then it "jumps" to a higher value (roughly an order of magnitude higher). The threshold-like value for G_{ex} decreases with increasing values of I_{app}, but the G_{ex}–f_{spk} curves remain abrupt-like. The voltage traces in Fig. 2-b correspond to values of G_{ex} on both sides of, and very close to, the abrupt transition.

For small enough values of I_{app} (small enough natural spike frequencies) the G_{ex}–f_{spk} curves in the IF model exhibit fast changes in f_{spk} (e.g., blue curve in Fig. 1-a1). However, as shown in [13], there are mechanistic differences between these and the abrupt transitions for the $I_h + I_{Nap}$ model, which are threshold like and present for a large range of values of natural frequencies.

3.2. Effects of synaptic delay on the modulation of the firing frequency transitions in self-connected cells

The effects of synaptic delay on neuronal dynamics are typically complex and not straightforward. This complexity is reflected in the dependence of f_{spk} on both I_{app} and G_{ex}. Figs. 1-a2 and -b2 illustrate this for the self-excited IF and $I_h + I_{Nap}$ cells with natural $f_{spk} = 10$ Hz (corresponding to the red curves in panels a1 and b1).

The dependence of the G_{ex}–f_{spk} curves on t_{del} are qualitatively similar for the two models, although the characteristic shapes corresponding to the two different modes of transition (gradual and abrupt) persist. For simplicity, below we describe this dependence only for the $I_h + I_{Nap}$ model.

Please cite this article in press as: C. Schindewolf et al., Complex patterns in networks of hyperexcitable neurons, Theoret. Comput. Sci. (2015), http://dx.doi.org/10.1016/j.tcs.2015.05.051

As t_{del} increases, the transition value for G_{ex} decreases, implying that the cells become more hyperexcitable. This is similar to the effect of increasing I_{app} (panel b1), but in contrast to it, f_{spk} jumps to a lower value the larger t_{del}.

The intersections between the G_{ex}–f_{spk} curves for different values of t_{del} indicate the existence of inversions in the relative magnitudes of f_{spk} for different values of t_{del} as G_{ex} increases. This implies that t_{del} has a non-monotonic effect on f_{spk}. For instance, for $G_{ex} = 0.22$ in Fig. 1-b2, an increase in t_{del} from $t_{del} = 0$ (blue curve) to $t_{del} = 1$ (red curve) causes an increase in f_{spk}, but a further increase to $t_{del} = 5$ (green curve) causes a decrease in f_{spk}.

Overall, these results show that synaptic delay contributes to the network hyperexcitability but also to stabilize the firing frequency at lower values in the high-frequency regime.

3.3. Synchronized patterns in recurrently connected two-cell networks: in-phase, antiphase and bistability

The network population frequency depends not only on the firing frequency of the individual neurons, but also on the network synchronization properties. Here we examine whether the effects described above for self-excited cells persist for networks of two-recurrently excited cells and the resulting patterns in the different frequency regimes. As a baseline case we consider parameter values such that $f_{spk} = 10$ Hz for the isolated cells (red curves in Figs. 1-a1 and -b1). Our results in Fig. 3 show that the IF and $I_h + I_{Nap}$ models show gradual and abrupt transitions respectively between firing frequency regimes as G_{ex} increases. However, in-phase patterns are not always stable. Specifically, depending on the values of G_{ex} and t_{del}, the two-cell networks may exhibit in-phase patterns, antiphase patterns or bistability between them.

For the IF model, the network synchronizes in-phase for low enough values of G_{ex} (Fig. 3-a1) and in antiphase for large enough values of G_{ex} (Fig. 3-a2). The spike alternation in the antiphase patterns cause f_{spk} to increase faster with increasing values of G_{ex} (compare panels a1 and a2) than it would for self-connected networks. An increase in t_{del} generates bistability between in-phase (Fig. 3-a3-i) and antiphase (Fig. 3-a3-ii) patterns. For the latter, the population frequency is slightly higher than for in-phase patterns, but not twice as much.

For the $I_h + I_{Nap}$ model, the network synchronizes in-phase in the low-frequency regime (Figs. 3-b1 and 3-b2-ii) and in antiphase in the high-frequency regime (Fig. 3-b2-i). For low enough values of G_{ex} the in-phase low-frequency patterns are the only stable patterns. For higher values of G_{ex} bistability arises between an antiphase high-frequency pattern (Fig. 3-b2-i) and an in-phase low-frequency pattern (Fig. 3-b2-ii). For larger values of G_{ex}, the antiphase high-frequency patterns are the only stable ones (not shown). As for the self-connected cells, the value of f_{spk} is almost independent of G_{ex} in the low-frequency regime.

Increasing values of t_{del} may cause f_{spk} to transition to a high-frequency regime (Fig. 3-b3). As in the self-connected cells, the firing frequency in the high-frequency regime is lower than for instantaneous synaptic connections. As in the IF model, there is bistability between in-phase (Fig. 3-b3-i) and antiphase (Fig. 3-b3-ii) patterns. However, in contrast to the IF model, the population frequency is almost the same. The lower value of f_{spk} as compared to Fig. 3-b2-i is due to the higher value of t_{del} and a slightly lower value of G_{ex}.

Together, these results show that the different modes of transition between firing frequency regimes described for self-connected cells persist in two-cell networks, but the ability of the cells to synchronize out-of-phase increases the complexity of the resulting patterns with potential implications for larger networks.

3.4. Dynamics of networks with ring-type architecture

Here we examine whether the effects described above for two-cell IF and $I_h + I_{Nap}$ networks persist in networks with a larger number of cells and what additional patterns emerge as a consequence of the larger dimensionality of the system. We consider networks having 10 cells and we focus on a ring architecture where each neuron is connected to its two nearest neighbors. As for the two-cell networks described above, we consider intrinsic parameter values such that the isolated cells fire with $f_{spk} = 10$ Hz. For each model type we used two (or sometimes three) representative values of G_{ex} that capture the key modes of behavior of the network dynamics and the differences between the two modes of transition.

In order to investigate the generation of stable activity patterns, for each representative set of parameter values we considered structured initial conditions (Figs. 4 to 7) where (i) all neurons fire sequentially following the order of their index number (neuron 1 fires first, neuron 2 fires second, etc.), and (ii) consecutive spikes in a given event (time window) are separated by equal time intervals, which we measure in terms of the phase $\Delta\phi_0$ (time interval normalized by the natural period). The smaller $\Delta\phi_0$, the shorter the IC support in the LFP graphs. Clearly, $\Delta\phi_0 = 0$ corresponds to all neurons initially synchronized in phase and $\Delta\phi_0 = (N-1)^{-1}$ corresponds to the neurons spanning the full period of the isolated cell. In addition to structured initial conditions, in Figs. 8 and 9 we used random initial conditions where the spike time for each neuron was drawn from a Gaussian distribution with mean t_0 and variance D.

We characterized the outputs in Figs. 4 to 9 by using the so-called raster plots (top panels) for the evolution of the spike times of all neurons in the network and the LFP graphs (bottom panels) for the evolution of the population activity using eq. (7). In the raster plots each spike time is indicated by a vertical line segment.

Please cite this article in press as: C. Schindewolf et al., Complex patterns in networks of hyperexcitable neurons, Theoret. Comput. Sci. (2015), http://dx.doi.org/10.1016/j.tcs.2015.05.051

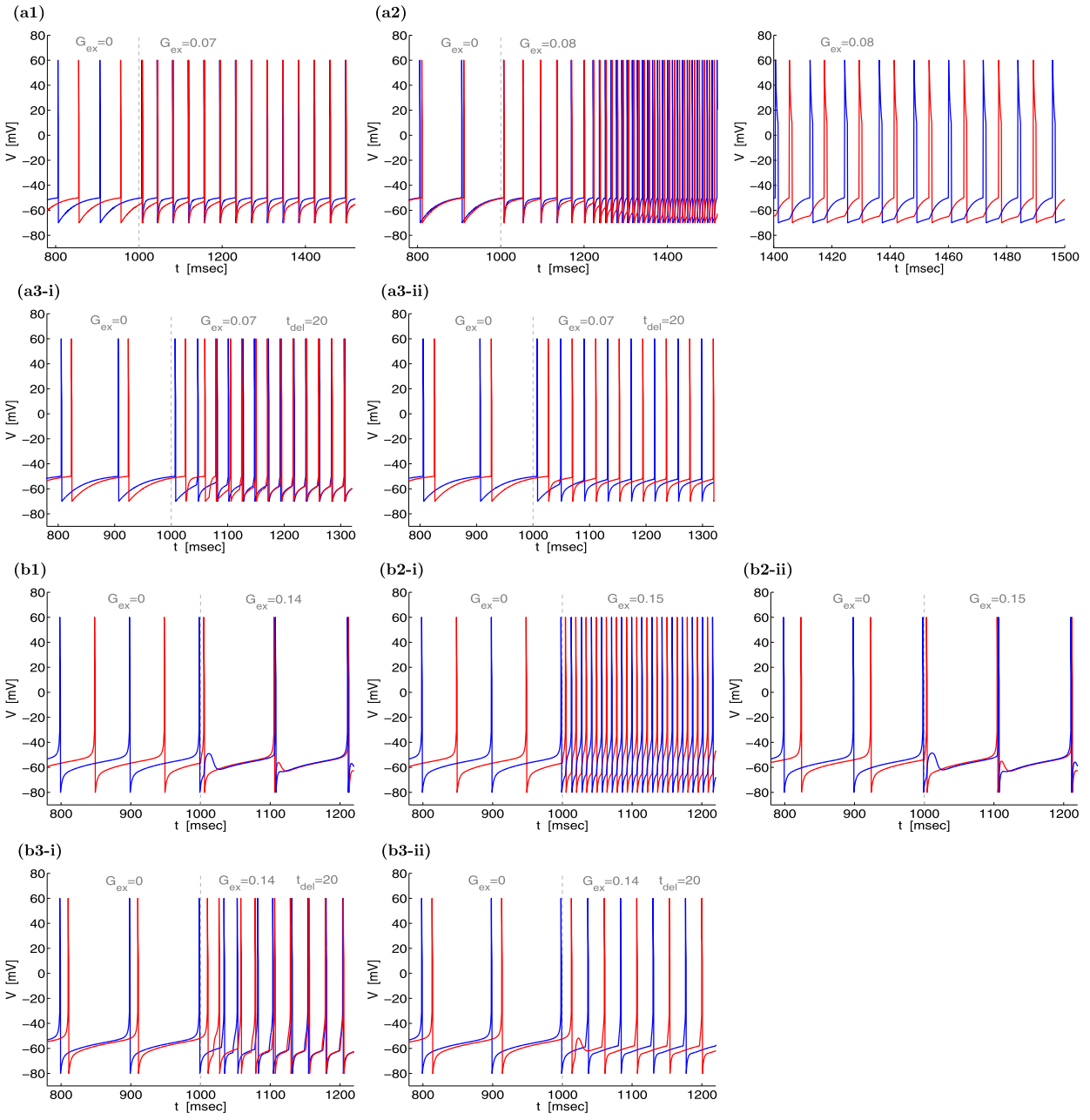

Fig. 3. Representative voltage traces for two-cell IF and $I_h + I_{Nap}$ network models before and after recurrent excitation is activated. The vertical gray line indicates the connection time. (a) IF model. We used the following parameter values $C = 1$, $E_L = -65$, $G_L = 0.025$, $I_{app} = 0.42$. a1 and a2. $t_{del} = 0$. a3. $t_{del} = 20$. (b) $I_h + I_{Nap}$ model. We used the following parameter values $C = 1$, $G_L = 0.5$, $G_h = 1.5$, $E_L = -65$, $E_{Na} = 55$, $E_h = -20$, $I_{app} = -1.78$. b1 and b2. $t_{del} = 0$. b3. $t_{del} = 20$.

3.4.1. IF networks with instantaneous recurrent AMPA excitation

Fig. 4 shows the behavior of IF networks with $t_{del} = 0$ for $G_{ex} = 0.035$ (panels a) and $G_{ex} = 0.04$ (panels b). For $\Delta\phi_0$ small enough and $G_{ex} = 0.035$ (panels a1 and a2) the network exhibits almost in-phase patterns with all neurons firing in very small time windows. A closer look into these patterns shows the presence of an "arrow head shaped" structure. Comparison between panels a1 and a2 shows that the population frequency of these patterns depends on the initial conditions. It increases with increasing values of $\Delta\phi_0$ within some range. For values of $\Delta\phi_0$ beyond that range (panel a3) the resulting patterns are wave-like, organized in oblique stripes at a much higher frequency for both the individual neurons and the population.

For $G_{ex} = 0.04$ (panels b) there is bistability between the patterns in panels b1 and b2. The steady pattern in panel b1 (inset) consists of two alternating arrow-head-shaped waves where the neurons are divided into two groups. Each neu-

Please cite this article in press as: C. Schindewolf et al., Complex patterns in networks of hyperexcitable neurons, Theoret. Comput. Sci. (2015), http://dx.doi.org/10.1016/j.tcs.2015.05.051

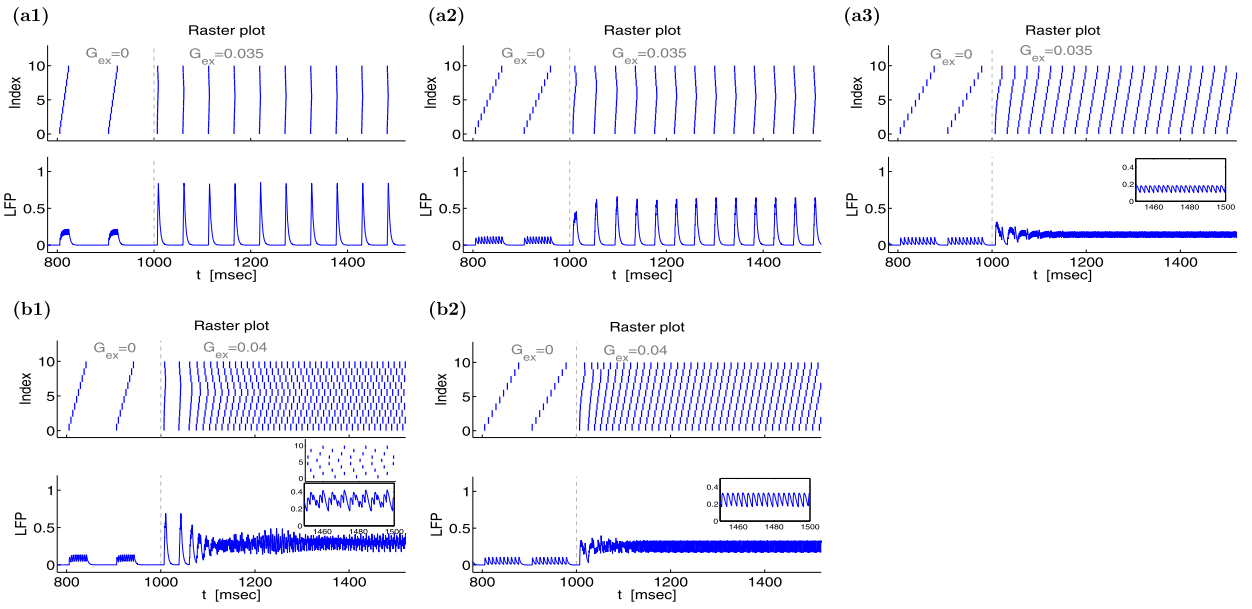

Fig. 4. Representative raster plots and LFP graphs for a network of ten IF neurons before and after recurrent excitation is activated. The vertical gray line indicates the connection time. a. $G_{ex} = 0.035$ and $t_{del} = 0$. b. $G_{ex} = 0.04$ and $t_{del} = 0$. We used the following parameter values $C = 1$, $E_L = -65$, $G_L = 0.025$, $I_{app} = 0.42$.

ron's nearest neighbors belong in a different group. All neurons in each group fire in a relatively small time window. The population pattern is irregular and consists roughly of two superimposed frequencies. Similar patterns are obtained for smaller values of $\Delta\phi_0$. However, the smaller $\Delta\phi_0$, the longer it takes for the network to reach the steady state pattern. The mechanism of desynchronization consists of the transition to a single "arrow head" wave-like pattern as in panel a2 and a subsequent transition into the alternating (steady) pattern (see inset). This last transition does not occur for $G_{ex} = 0.035$ (panel a2), that is why there is a rather big change in the population frequency between panels a2 and b1. The pattern in panel b2, corresponding to a larger value of $\Delta\phi_0$, consists of wave-like oblique stripes, similar to the pattern in panel a3 but at a higher population frequency. The increase in firing frequency between panels a3 and b2 is gradual. Note also that within the two types of patterns the frequency for both the individual neurons and the population may change depending on initial conditions.

3.4.2. $I_h + I_{Nap}$ networks with instantaneous recurrent AMPA excitation

Fig. 5 shows the behavior of $I_h + I_{Nap}$ networks for three values of G_{ex}: $G_{ex} = 0.08$ (panels a), $G_{ex} = 0.1$ (panels b) and $G_{ex} = 0.12$ (panels c) and $t_{del} = 0$. For low enough values of G_{ex} (panels a and b) there is bistability between the low-frequency quasi-in-phase patterns (left) and the wave patterns (right). In the wave patterns, each neuron fires at low frequencies, but the population frequency is much higher. For higher values of G_{ex} (panels c) there is bistability between the high-frequency quasi-antiphase patterns (left) and the wave patterns (right). In both cases the population frequency is very high, but for different reasons. The transition from the low- to the high-frequency patterns in the left panels is abrupt and corresponds to the abrupt transitions observed for the self-connected cells and two-cell networks discussed above. The emergence of the fast time scale is already reflected in the low-frequency bursts in panel b1. For higher values of G_{ex} ($\in [0.14, 0.15]$) an abrupt transition between the wave and high-frequency patterns occurs (not shown) and bistability disappears.

3.4.3. IF networks with delayed recurrent AMPA excitation

We now examine the effects of synaptic delay on the patterns discussed in Section 3.4.1 for $t_{del} = 0$. In Fig. 6 we use the same parameter values ($G_{ex} = 0.035$ and $G_{ex} = 0.04$) as in Fig. 4 with $t_{del} = 10$ (panels a and c) and $t_{del} = 20$ (panels b and d). Overall, synaptic delay decreases both the individual cells and population firing frequency and generates more regular patterns.

For $t_{del} = 10$ the network patterns are bistable for both $G_{ex} = 0.035$ (panels a) and $G_{ex} = 0.04$ (panels b). The network synchronizes in phase for very small values of $\Delta\phi_0$ (panels a1 and c1) and in antiphase for larger values of $\Delta\phi_0$ (panels a2 and c2). The antiphase patterns consist of alternating clusters. Each cluster consists of half the neurons with their nearest neighbors belonging in a different cluster. Within each cluster the neurons are synchronized in phase. Synchronization within a cluster is better than for $t_{del} = 0$ (compare with Fig. 4-b2). As expected, the firing frequencies of both the individual neurons and the population increase with increasing values of G_{ex}. For $t_{del} = 20$ the network patterns synchronize in phase

Please cite this article in press as: C. Schindewolf et al., Complex patterns in networks of hyperexcitable neurons, Theoret. Comput. Sci. (2015), http://dx.doi.org/10.1016/j.tcs.2015.05.051

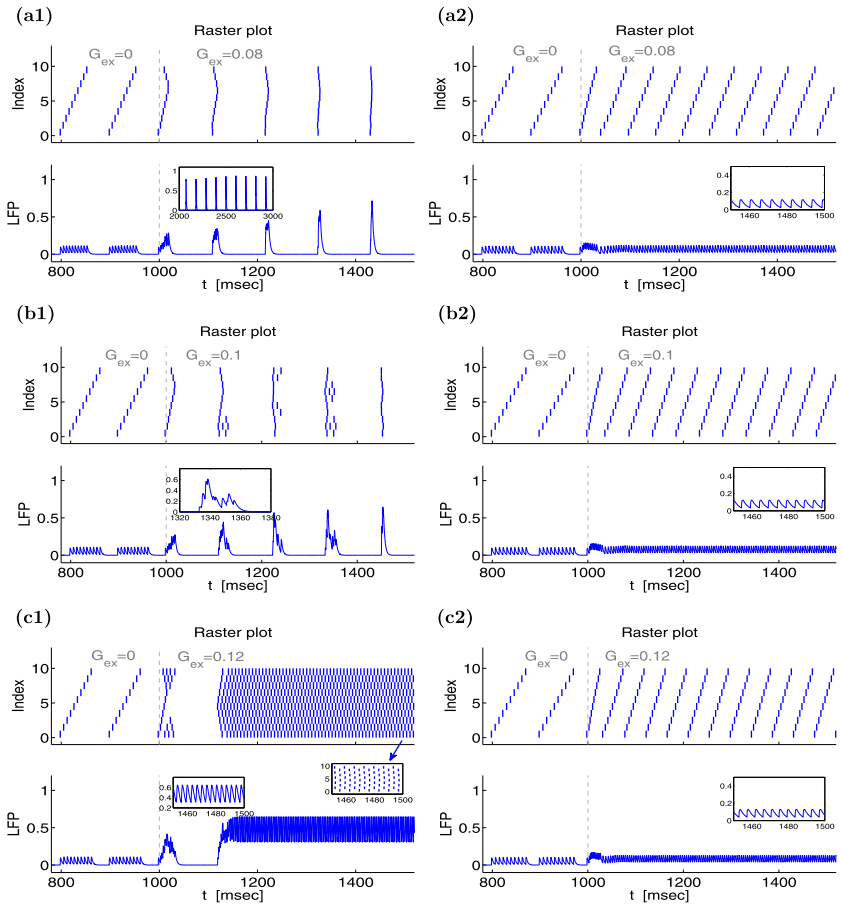

Fig. 5. Representative raster plots and LFP graphs for a network of ten $I_h + I_{Nap}$ neurons before and after recurrent excitation is activated. The vertical gray line indicates the connection time. a. $G_{ex} = 0.08$ and $t_{del} = 0$. b. $G_{ex} = 0.1$ and $t_{del} = 0$. c. $G_{ex} = 0.12$ and $t_{del} = 0$. We used the following parameter values $C = 1$, $G_L = 0.5$, $G_h = 1.5$, $E_L = -65$, $E_{Na} = 55$, $E_h = -20$, $I_{app} = -1.78$.

(panels b and d) regardless of their initial conditions. Both the individual neurons and the population frequencies are smaller than for $t_{del} = 10$.

3.4.4. $I_h + I_{Nap}$ networks with delayed recurrent AMPA excitation

We now turn to discuss the effect of synaptic delay on the patterns discussed in Section 3.4.2 for the $I_h + I_{Nap}$ model with $t_{del} = 0$. Our results are presented in Fig. 7. We use the same parameter values ($G_{ex} = 0.08$ and $G_{ex} = 0.12$) as in Fig. 5 with $t_{del} = 10$ (panels a and c) and $t_{del} = 20$ (panels b and d).

For $G_{ex} = 0.08$ the network exhibits antiphase cluster patterns for both $t_{del} = 10$ (panel a) and $t_{del} = 20$ (panel b). Both the individual cells and population frequencies are smaller for $t_{del} = 20$ (panel b) than for $t_{del} = 10$ (panel a). However, comparison between these figures and Fig. 5-a show that the firing frequencies for these values of t_{del} are larger than for $t_{del} = 0$ for the in-phase patterns (panel a1). In contrast, for the wave patterns (panel a2) the population frequency is larger for $t_{del} = 0$ than for $t_{del} = 10$ and $t_{del} = 20$.

For $G_{ex} = 0.12$ the network exhibits antiphase cluster patterns for $t_{del} = 10$ (panel c) and quasi-in-phase patterns for $t_{del} = 20$ (panel d) with no bistability in either case. As before, the frequencies of both the individual neurons and the population are smaller for $t_{del} = 20$ than for $t_{del} = 10$. Comparison with Fig. 5-c shows that in contrast to when $G_{ex} = 0.08$, increasing values of t_{del} decrease the firing frequencies for both the individual oscillators and the population in the high-frequency regime. Still, there is an abrupt transition between the low and high frequency regimes.

3.4.5. Pattern selection for noisy initial conditions

In Figs. 8 and 9 we illustrate the patterns obtained for both the IF (Fig. 8) and $I_h + I_{Nap}$ (Fig. 9) models using noisy initial conditions for a representative value of the variance D that creates an intermediate sized IC support. The values of G_{ex} and t_{del} are as in the previous figures. For both models, the patterns obtained are similar to the ones discussed before for the structured (not noisy) initial conditions.

Please cite this article in press as: C. Schindewolf et al., Complex patterns in networks of hyperexcitable neurons, Theoret. Comput. Sci. (2015), http://dx.doi.org/10.1016/j.tcs.2015.05.051

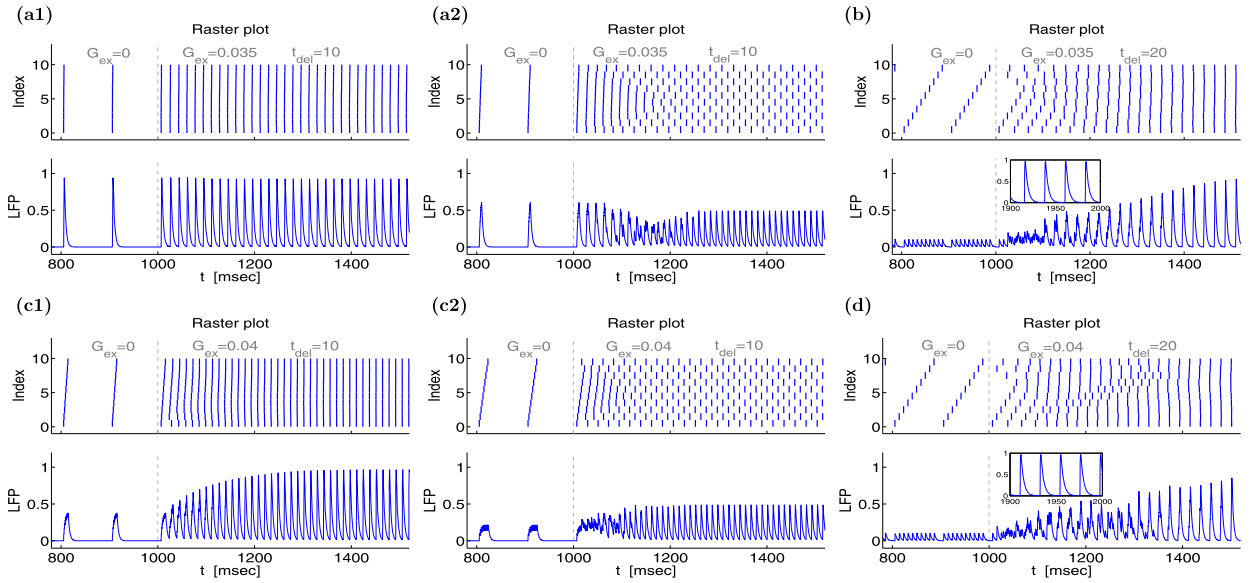

Fig. 6. Representative raster plots and LFP graphs for a network of ten IF neurons before and after recurrent excitation is activated. The vertical gray line indicates the connection time. a. $G_{ex} = 0.035$ and $t_{del} = 10$. b. $G_{ex} = 0.035$ and $t_{del} = 20$. c. $G_{ex} = 0.04$ and $t_{del} = 10$. d. $G_{ex} = 0.04$ and $t_{del} = 20$. We used the following parameter values $C = 1$, $E_L = -65$, $G_L = 0.025$, $I_{app} = 0.42$.

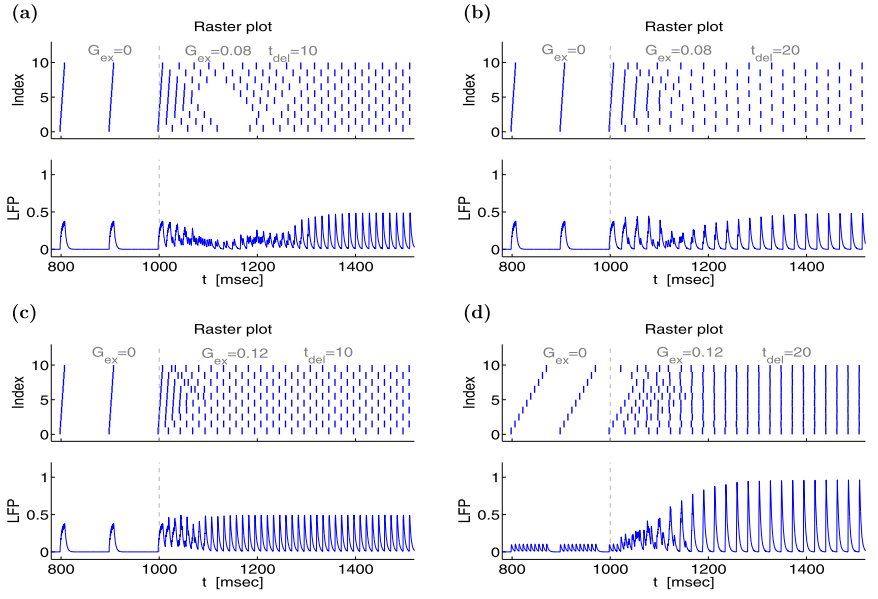

Fig. 7. Representative raster plots and LFP graphs for a network of ten $I_h + I_{Nap}$ neurons before and after recurrent excitation is activated. The vertical gray line indicates the connection time. a. $G_{ex} = 0.08$ and $t_{del} = 10$. b. $G_{ex} = 0.08$ and $t_{del} = 20$. c. $G_{ex} = 0.1$ and $t_{del} = 10$. d. $G_{ex} = 0.12$ and $t_{del} = 20$. We used the following parameter values $C = 1$, $G_L = 0.5$, $G_h = 1.5$, $E_L = -65$, $E_{Na} = 55$, $E_h = -20$, $I_{app} = -1.78$.

For the IF model and $G_{ex} = 0.035$ (Fig. 8-a), an increase in t_{del} to $t_{del} = 10$ desynchronizes the network pattern and increases the network frequency (panel a2). A further increase to $t_{del} = 20$ regenerates the in-phase network pattern and decreases the network frequency. The reduction in the network frequency is due to both a decrease in the individual neurons spiking frequency and the generation of in-phase patterns. For $G_{ex} = 0.04$ (Fig. 8-b), the effects of delay are more significant since for $t_{del} = 0$ the population frequency is very high compared to Fig. 8-a1.

For the $I_h + I_{Nap}$ model and $G_{ex} = 0.1$ (low frequency regime, Fig. 9-a) an increase in t_{del} to $t_{del} = 10$ desynchronizes the network pattern and increases the network frequency (panel a2) as in the IF model. However, in contrast to the IF model, a further increase to $t_{del} = 20$ does not regenerate the in-phase patterns. Despite this, the network frequency decreases as a result of a decrease in the firing frequency of the individual cells. For $G_{ex} = 0.12$ (high frequency regime, Fig. 9-b) an increase in t_{del} decreases the network frequency by reducing the firing frequency of the individual neurons without

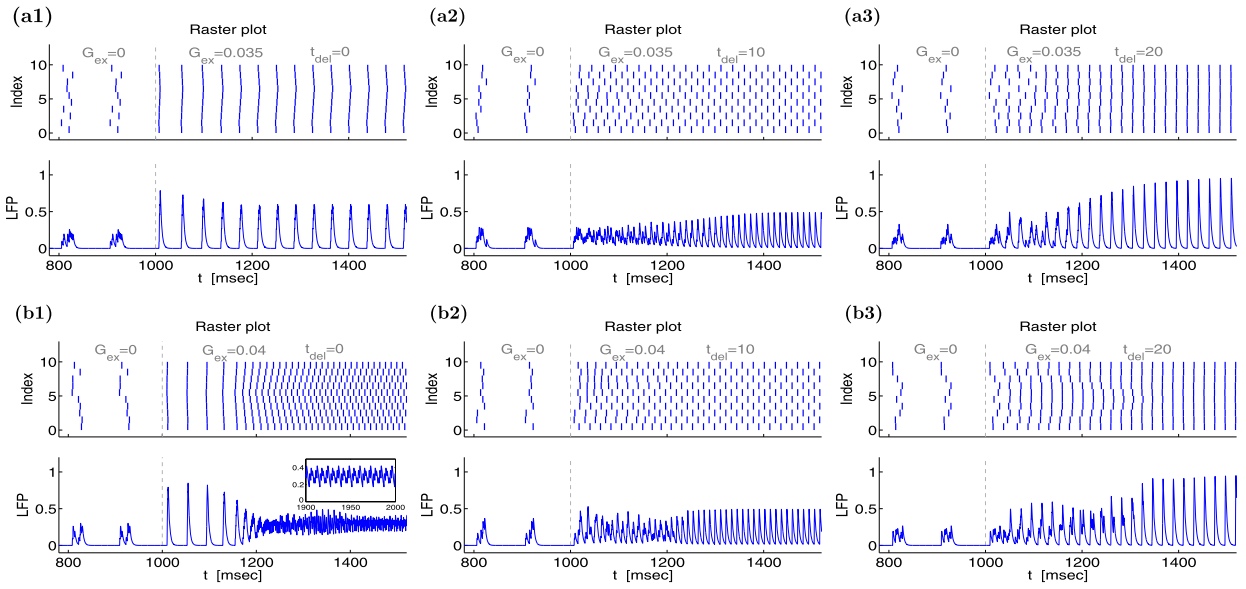

Fig. 8. Representative raster plots and LFP graphs for a network of ten IF neurons before and after recurrent excitation is activated for random initial conditions. The vertical gray line indicates the connection time. a. $G_{ex} = 0.035$. b. $G_{ex} = 0.04$. We used the following parameter values $C = 1$, $E_L = -65$, $G_L = 0.025$, $I_{app} = 0.42$ and $D = 25$.

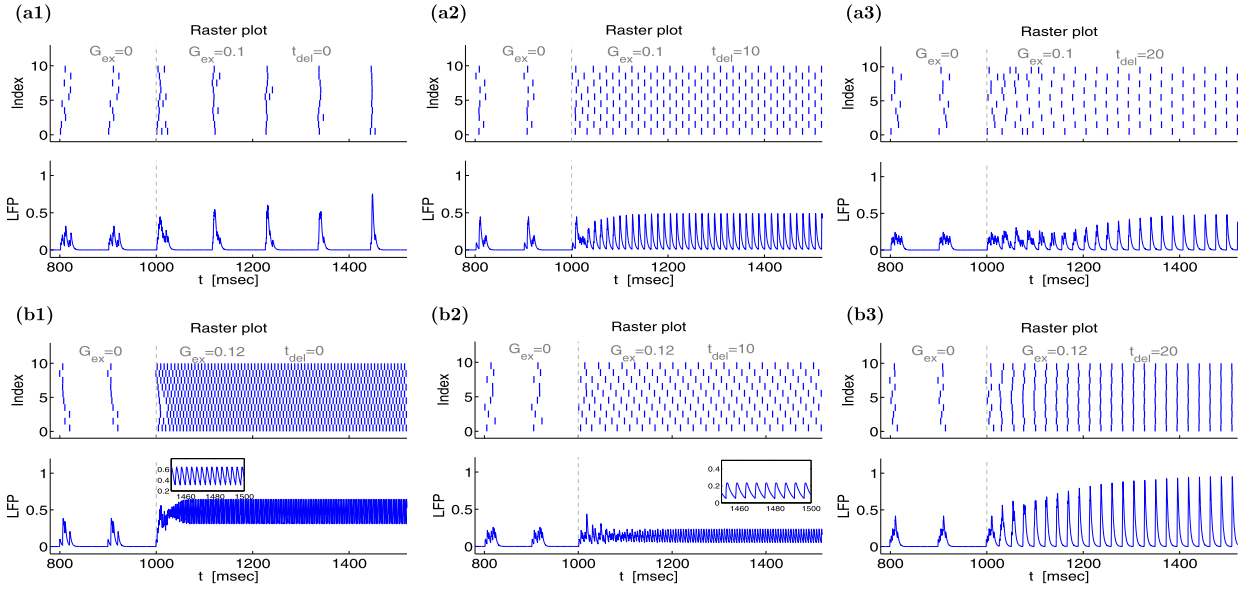

Fig. 9. Representative raster plots and LFP graphs for a network of ten $I_h + I_{Nap}$ neurons before and after recurrent excitation is activated for random initial conditions. The vertical gray line indicates the connection time. a. $G_{ex} = 0.1$. b. $G_{ex} = 0.12$. We used the following parameter values $C = 1$, $G_L = 0.5$, $G_h = 1.5$, $E_L = -65$, $E_{Na} = 55$, $E_h = -20$, $I_{app} = -1.78$ and $D = 25$.

necessarily generating a regular synchronized pattern ($t_{del} = 10$, panel b2) and by regenerating an in-phase synchronized pattern ($t_{del} = 20$, panel c2).

4. Discussion

In this paper we have extended previous results [12,13] on the mechanisms of transition between low and high firing frequencies in recurrently connected networks via AMPA excitation. We have used two types of neuron models: IF and $I_h + I_{Nap}$. We have previously shown that they exhibit gradual and abrupt transitions between firing frequency regimes respectively in self-excited networks mimicking recurrently connected networks synchronized in phase [13].

Please cite this article in press as: C. Schindewolf et al., Complex patterns in networks of hyperexcitable neurons, Theoret. Comput. Sci. (2015), http://dx.doi.org/10.1016/j.tcs.2015.05.051

The main biophysical difference between the two models lies in the description of the ionic currents present in the subthreshold regime. The IF model lacks any active ionic current and displays only passive behavior in the subthreshold voltage regime. The $I_h + I_{Nap}$ model, in contrast, includes a persistent sodium current and an h-current in addition to the leak current, and therefore displays more complex subthreshold behavior. From the dynamic point of view, the IF model is linear and one-dimensional, while the $I_h + I_{Nap}$ model is nonlinear, two-dimensional and has a significant time scale separation between the voltage and the h-current gating variable [49]. The ability of the $I_h + I_{Nap}$ model to remain in the low firing frequency regime and have a non-increasing firing frequency for a significantly large range of values of G_{ex} results from this complex subthreshold dynamic structure [13].

We set out to examine whether the gradual and abrupt transitions observed in minimal recurrently connected network models persist in networks with a larger number of cells, what are the patterns that emerge in these models, what are the similarities and differences of these patterns for the two different model types, and what are the effects of synaptic delay on the network patterns. The relatively simple ring topology we used is appropriate to begin to investigate these questions. More research is needed to extend our results to more complex network architectures (e.g., all-to-all, small-world) and compare the results using models such as the $I_h + I_{Nap}$ model with the IF and the Hodgkin–Huxley model used in [7–11].

Our results show that the properties of the minimal $I_h + I_{Nap}$ network models are communicated to the network level. Specifically, $I_h + I_{Nap}$ network models exhibit abrupt transitions between population frequency regimes, and the population frequency remains almost constant for significantly large ranges of values of G_{ex} in the low frequency regime. In the latter, neurons are almost synchronized in phase by firing in very small time windows. However, these networks are bistable. When the initial spiking distribution is highly spread out, traveling waves develop and the low population frequency regime no longer exists. The traveling waves frequency is larger than the population frequency in the low-frequency regime (around twice as large), but still roughly the same order of magnitude. This reflects the existence of an additional time scale where the individual neurons fire faster than they do in the low-frequency regime but well below their firing frequency in the high-frequency regime. This time scale is not present in self-excited cells or two-cell networks, and the underlying mechanism is expected to be strongly dependent on the network connectivity and topology. In the high-frequency regime, neurons do not synchronize in-phase but in alternating antiphase patterns.

Our results also show the complex effects of synaptic delay for network dynamics. Even for self-excited networks, increasing values of synaptic delay can cause the abrupt transitions between firing frequency to occur for lower transition G_{ex} values, but to a lower frequency value. In addition, for fixed-values of G_{ex} the firing frequency first increases and then decreases with increasing values of synaptic delay. This is communicated to the network level in various ways. For the cases we studied here, increasing values of synaptic delay cause a decrease in the population frequency by various mechanisms that included synchronization in phase and in antiphase. These effects and mechanisms are shared by networks of both IF and $I_h + I_{Nap}$ models. However, here we have considered a very small set of delay values. Differences between the two models may have remained uncovered. More generally, although our results are valid for larger parameter sets and seem to be independent of the neuron type, more research is needed both to establish the effects of synaptic delay in more complex networks and to unravel the underlying mechanisms. We would like to note that while we have observed only bistability, the possibility remains open for the existence of additional stable states in both regimes. Some of these stable states may lead to similar population frequencies.

The focus of this paper was excitatory networks. Future work should include the effect of inhibitory neurons to test the hypothesis that inhibition acts as a switch between the low- and high-frequency regimes, and thus maintains a net balance between excitation and inhibition necessary for healthy network activity.

The switching between firing frequency regimes investigated in this paper is expected to have consequences for neuronal computations in larger networks. More research is needed to identify these computational properties.

Acknowledgements

This work was partially funded by the NSF grant DMS-1313861 (HGR) and a travel grant awarded by Universidad Nacional del Sur (Bahía Blanca, Buenos Aires, Argentina) to AB (Res. CSU-749/13 and PGI 24/L085).

References

[1] E. Bullmore, O. Sporns, Complex brain networks: graph theoretical analysis of structural and functional systems, Nat. Rev. Neurosci. 10 (2009) 186–198.
[2] G. Buzsáki, Rhythms of the Brain, Oxford University Press, 2006.
[3] X.J. Wang, Neurophysiological and computational principles of cortical rhythms in cognition, Physiol. Rev. 90 (2010) 1195–1268.
[4] G.B. Ermentrout, D. Terman, Mathematical Foundations of Neuroscience, Springer, 2010.
[5] P.E. Sharp, H.T. Blair, J. Cho, The anatomical and computational basis of the rat head-direction cell signal, Trends Neurosci. 24 (2001) 289–294.
[6] J.J. Knierim, K. Zhang, Attractor dynamics of spatially correlated neural activity in the limbic system, Annu. Rev. Neurosci. 32 (2012) 267–285.
[7] T.I. Netoff, R. Clewley, S. Arno, T. Keck, J.A. White, Epilepsy in small-world networks, J. Neurosci. 24 (2004) 8075–8083.
[8] A. Roxin, H. Riecke, S.A. Solla, Self-sustained activity in a small-world network of excitable neurons, Phys. Rev. Lett. 92 (2004) 198101.
[9] H. Riecke, A. Roxin, S. Madruga, S.A. Solla, Multiple attractors, long chaotic transients, and failure in small world networks of excitable neurons, Chaos 17 (2007) 026110.
[10] L.F. Lago-Fernández, R. Huerta, F. Corbacho, J.A. Siguenza, Fast response and temporal coherent oscillations in small-world networks, Phys. Rev. Lett. 84 (2000) 2758–2761.
[11] L.F. Lago-Fernández, F. Corbacho, R. Huerta, Connection topology dependence of synchronization of neural assemblies on class 1 and 2 excitability, Neural Netw. 14 (2001) 687–696.

Please cite this article in press as: C. Schindewolf et al., Complex patterns in networks of hyperexcitable neurons, Theoret. Comput. Sci. (2015), http://dx.doi.org/10.1016/j.tcs.2015.05.051

[12] T. Kispersky, J.A. White, H.G. Rotstein, The mechanism of abrupt transition between theta and hyperexcitable spiking activity in medial entorhinal cortex layer II stellate cells, PLoS One 5 (2010) e13697.
[13] H.G. Rotstein, Abrupt and gradual transitions between low and hyperexcited firing frequencies in neuronal models with fast synaptic excitation: a comparative study, Chaos 23 (2013) 046104.
[14] C.E. Stafstrom Epilepsy, A review of selected clinical syndromes and advances in basic science, J. Cereb. Blood Flow Metab. 26 (2006) 983–1004.
[15] L. El-Hassar, M. Esclapez, C. Bernard, Hyperexcitability of the ca1 hippocampal region during epileptogenesis, Epilepsia 48 (2007) 131–139.
[16] R.S. Sloviter, Decreased hippocampal inhibition and a selective loss of interneurons in experimental epilepsy, Science 235 (1987) 73–76.
[17] J.W. Bekenstein, E.W. Lothman, Dormancy of inhibitory interneurons in a model of temporal lobe epilepsy, Science 259 (1993) 97–100.
[18] F. Du, T. Eid, E.E. Lothman, C. Køler, R. Schwarcz, Preferential neuronal loss in layer III of the medial entorhinal cortex in rat models of temporal lobe epilepsy, J. Neurosci. 15 (1995) 6301–6313.
[19] J. Bear, N.B. Fountain, E.W. Lothman, Responses of superficial entorhinal cortex in vitro slices from naive and chronically epileptic rats, J. Neurophysiol. 76 (1996) 2928–2940.
[20] T. Eid, R. Schwarcz, O.P. Ottersen, Ultrastructure and immunocytochemical distribution in layer III of the rat medial entorhinal cortex following aminooxyacetic acid-induced seizures, Exp. Brain Res. 125 (1999) 463–475.
[21] R. Schwarcz, E. Tore, F. Du, Neurons in layer III of the entorhinal cortex: a role in epileptogenesis and epilepsy?, Ann. N.Y. Acad. Sci. 911 (2000) 328–342.
[22] E.A. Tolner, F. Klosterman, E.A. van Vliet, M.P. Witter, F.H. Lopes da Silva, J.A. Gorter, Presubiculum stimulation in vivo evokes distinct oscillations in superficial and deep entorhinal cortex layers in chronic epileptic rats, J. Neurosci. 25 (2005) 8755–8765.
[23] S.S. Kumar, P.S. Buckmaster, Hyperexcitability, interneurons, and loss of GABAergic synapses in entorhinal cortex in a model of temporal lobe epilepsy, J. Neurosci. 26 (2006) 4613–4623.
[24] S. Abbasi, S.S. Kumar, Regular-spiking cells in the presubiculum are hyperexcitable in a rat model of temporal lob epilepsy, J. Neurophysiol. 112 (2014) 2888–2900.
[25] J.V. Nadler, The recurrent mossy fiber pathway of the epileptic brain, Neurochem. Res. 28 (2003) 169–1658.
[26] V. Santhakumar, I. Aradi, I. Soltesz, Role of mossy fiber sprouting and mossy cell loss in hyperexcitability: a network model of the dentate gyrus incorporating cell types and axonal topography, J. Neurophysiol. 93 (2005) 437–453.
[27] G. Golarai, A.C. Greenwood, D.M. Feeney, J.A. Connor, Physiological and structural evidence for hippocampal involvement in persistent seizure susceptibility after traumatic brain injury, J. Neurosci. 21 (2001) 8523–8537.
[28] V. Santhakumar, A.D. Ratzliff, J. Jeng, K. Toth, I. Soltesz, Long-term hyperexcitability in the hippocampus after experimental head trauma, Ann. Neurol. 50 (2001) 708–717.
[29] D.A. Coulter, Chronic epileptogenetic cellular alterations in the limbic system after status epilepticus, Epilepsia 40 (1999) S23–S33.
[30] T.P. Sutula, G. Golarai, J. Cavazos, Assessing the functional significance of mossy fiber sprouting, Epilepsy Res. Suppl. 7 (1992) 251–259.
[31] W. Zhang, J.R. Huguenard, P.S. Buckmaster, Increased excitatory synaptic input to granule cell from hilar and ca3 regions in a rat model of temporal lobe epilepsy, J. Neurosci. 32 (2012) 1183–1196.
[32] J.M. Parent, D.H. Lowenstein, Mossy-fiber reorganization in the epileptic hippocampus, Curr. Opin. Neurobiol. 10 (1997) 103–109.
[33] T.N. Lehmann, S. Gabriel, A. Eilers, M. Njunting, R. Kovacs, K. Schulze, W.R. Lanksch, U. Heinemann, Fluorescent tracer in pilocarpine-treated rats shows widespread aberrant hippocampal neuronal connectivity, Eur. J. Neurosci. 14 (2001) 83–95.
[34] P. Salin, G.-F. Tseng, S. Hoffman, I. Parada, D.A. Prince, Axonal sprouting in layer V pyramidal neurons of chronically injured cerebral cortex, J. Neurosci. 15 (1995) 8234–8245.
[35] Y. Perez, F. Morin, C. Beaulieu, J.-C. Lacaille, Axonal sprouting of CA1 pyramidal cells in hyperexcitable hippocampal slices of kainate-treated rats, Eur. J. Neurosci. 8 (1996) 736–748.
[36] J. Drover, J. Rubin, J. Su, B. Ermentrout, Analysis of a canard mechanism by which excitatory synaptic coupling can synchronize neurons at low firing frequencies, SIAM J. Appl. Math. 65 (2004) 69–92.
[37] J. Rubin, Surprising effects of synaptic excitation, J. Comput. Neurosci. 18 (2005) 333–3423.
[38] S.S. Kumar, X. Jin, P.S. Buckmaster, J.R. Huguenard, Recurrent circuits in layer II of medial entorhinal cortex in a model of temporal lobe epilepsy, J. Neurosci. 27 (2007) 1239–1246.
[39] N. Kopell, G.B. Ermentrout, M. Whittington, R.D. Traub, Gamma rhythms and beta rhythms have different synchronization properties, Proc. Natl. Acad. Sci. USA 97 (2000) 1867–1872.
[40] S. Weiss, H.M. Mueller, Too many betas do not spoil the broth: the role of beta brain oscillations in language processing, Front. Psychol. 3 (2012) 201.
[41] M. Bartos, I. Vida, M. Frotscher, A. Meyer, H. Monyer, J.R. Geiger, P. Jonas, Fast synaptic inhibition promotes synchronized gamma oscillations in hippocampal interneuron networks, Proc. Natl. Acad. Sci. USA 99 (2002) 13222–13227.
[42] I. Vida, M. Bartos, P. Jonas, Shunting inhibition improves robustness of gamma oscillations in hippocampal interneuron networks by homogenizing firing rates, NEURON 49 (2006) 107–117.
[43] A. Arenas, A. Díaz-Guilera, J. Kurths, Y. Moreno, C. Zhou, Synchronization in complex networks, Phys. Rep. 469 (2008) 93–153.
[44] B.G. Ermentrout, N. Kopell, Fine structure of neural spiking and synchronization in the presence of conduction delays, Proc. Natl. Acad. Sci. USA 95 (1998) 1259–1264.
[45] W.W. Lytton, M. Stewart, M. Hines, Simulation of large networks: technique and progress, in: I. Soltesz, K. Staley (Eds.), Computational Neuroscience in Epilepsy, Elsevier, 2008.
[46] A. Bibbig, R. Traub, M. Whittington, Long-range synchronization of gamma and beta oscillations and the plasticity of excitatory and inhibitory synapses: a network model, J. Neurophysiol. 88 (2002) 1634–1654.
[47] J.J. Fox, C. Jayaprakash, D.L. Wang, S.R. Campbell, Synchronization in relaxation oscillator networks with conduction delays, Neural Comput. 13 (2001) 1003–1021.
[48] A.L. Hodgkin, A.F. Huxley, A quantitative description of membrane current and its application to conductance and excitation in nerve, J. Physiol. 117 (1952) 500–544.
[49] H.G. Rotstein, T. Oppermann, J.A. White, N. Kopell, A reduced model for medial entorhinal cortex stellate cells: subthreshold oscillations, spiking and synchronization, J. Comput. Neurosci. 21 (2006) 271–292.
[50] C.D. Acker, N. Kopell, J.A. White, Synchronization of strongly coupled excitatory neurons: relating network behavior to biophysics, J. Comput. Neurosci. 15 (2003) 71–90.

Please cite this article in press as: C. Schindewolf et al., Complex patterns in networks of hyperexcitable neurons, Theoret. Comput. Sci. (2015), http://dx.doi.org/10.1016/j.tcs.2015.05.051